Journal of CO2 Utilization 69 (2023) 102401

Contents lists available at ScienceDirect

Journal of CO2 Utilization

journal homepage: www.elsevier.com/locate/jcou

Spider silk-derived nanoporous activated carbon fiber for CO_2 capture and CH_4 and H_2 storage

Raeesh Muhammad [a], Yoon-Chae Nah [b], Hyunchul Oh [a,c,*]

[a] Department of Chemistry, Ulsan National Institute of Science and Technology, Ulsan 44919, Republic of Korea
[b] Future Convergence Engineering, School of Energy, Materials, and Chemical Engineering, Korea University of Technology and Education (KOREATECH), Cheonan 31253, Republic of Korea
[c] Graduate School of Carbon Neutrality, Ulsan National Institute of Science and Technology, Ulsan 44919, Republic of Korea

ARTICLE INFO

Keywords:
Nanoporous carbon fiber
CO_2 capture
Hierarchical porosity
CH_4 and H_2 storage

ABSTRACT

High surface area porous carbon with fibrous microstructure offers a broader application potential than powder form. However, controlling the microstructure with high porosity is difficult, and if possible then through a complex and time-consuming synthesis method. Herein, the development of high surface area nanoporous activated carbon fiber by activating spider silk (natural biomaterials) using potassium hydroxide is being reported. The specific surface area (SSA) and total pore volume for the developed material were 2730 m^2/g and 1.56 cc/g, respectively, and its surface contain high oxygen content. Its high SSA and oxygen-rich surface provide an enhanced CO_2 capture and energy carrier gases (H_2 and CH_4) storage capacity. The CO_2 capture capacity at 0 °C and 25 °C, 25 bar, were estimated to be 23.6 and 15.4 mmol/g, respectively, among the highest reported values for porous carbon fiber. Moreover, the developed sample has shown the CH_4 storage capacity of 8.6 mmol/g at 0 °C, 25 bar, and for H_2, it was 4.1 wt% at − 196 °C, 25 bar. In addition, the developed carbon material demonstrated an easy regeneration and almost negligible loss in uptake capacity, confirmed by adsorption-desorption cycles. The observation of high porosity and promising gas storage and recyclability in spider silk-derived activated carbon fiber indicates that the employed method can effectively convert biomaterials into high surface area activated carbon fibers for advanced energy and environmental applications.

1. Introduction

Carbonaceous porous materials have gained significant interest, given their prevalent use for energy and environmental applications [1–3]. The popularity of porous carbonaceous materials has mainly been driven by their easier preparation and scalability, robustness, high surface area, and simpler modulation of physicochemical properties [3–5]. The gas storage and separation in porous materials are primarily affected by the porosity and chemical environment of the pores [6–9]. To increase the gas storage and separation performance of carbonaceous materials, the textural properties are tuned by physical or chemical activation method, and the chemical environment of the internal surface is modulated by the introduction of hetero-atoms in the pores by post-synthesis modification or using the heteroatoms containing precursors [1–5,10]. The usage of heteroatom-containing precursors better tunes the pore chemistry as the distribution of the hetero atoms is uniform compared to post-synthesis modification which leads to non-homogeneous distribution. In this direction, biomaterials' utilization, as they contain the heteroatoms, has significant socio-economic advantages due to their renewability, cheapness, and vast availability [11],[12].

The utilization of biomaterials for the development of carbon materials has been used for a long time. Various carbon nanostructures like - carbon nanosheet [13], carbon foam [14], carbon aerogel [15], nano-onion [16], activated carbon fibers (ACFs) [17] and carbon in powder form [18] have been developed. Among these, ACFs are easy to handle and possess a unique fibrous structure, high porosity, and fast adsorption kinetics. These features of ACFs translate into improved performance in gas uptake, water purification, and volatile organic contaminant removal [11]. ACFs are conventionally synthesized by a time-consuming methodology combining electrospinning, followed by stabilization, carbonization, and activation [11], [19], [20]. Thus produced ACFs, due to long production time and low yield, can be applied for lab-scale studies only, and bulk synthesis for commercial application

* Corresponding author at: Department of Chemistry, Ulsan National Institute of Science and Technology, Ulsan 44919, Republic of Korea.
E-mail address: hcoh@unist.ac.kr (H. Oh).

https://doi.org/10.1016/j.jcou.2023.102401
Received 9 October 2022; Received in revised form 28 December 2022; Accepted 12 January 2023
Available online 16 January 2023

is still the issue. Hence, to meet the increased demand for ACFs, due to their suitability in various industrial applications, there is a need for a facile ACF synthesis approach.

ACFs are conventionally produced using polyacrylonitrile, phenolic resin and cellulosic biomass [20–22]. However, biomasses like cotton, jute, wood, coconut fiber, etc., due to the renewability factor, have gained much importance as a precursor for the synthesis of ACFs [23–26]. The hetero-atomic nature of biomass enables the development of ACFs having pores decorated with a heteroatom, and towards tuning the chemical nature of the pores, these also eliminate the need for post-synthesis modification. The conversion of biomass into ACFs involves activating these, which can be achieved by physical or chemical activation. However, the advantages, like better distribution of micropores and low activation temperature, make chemical activation more suitable for making ACFs. In chemical activation, KOH is one of the most explored activators as it mainly produces microporous ACFs and enhances the oxygen content. Huand et al. converted the wood sawdust into ACFs using KOH and studied the energy storage behavior. [25] Similarly, Zhang et al. employed KOH activation to convert coconut fibers into ACFs, and studied the removal of dye from water.[26] This shows that KOH activation of biomass for ACFs production will better attain sustainability in materials development.

Herein, we report the development of nanoporous-activated carbon fiber by chemical activation of spider silk using KOH. Spider silk is a natural polymer of Spidroins protein (which contains the hetero atoms) and possesses a fibrous structure [27]. Previously, Zhou et al. used spider silk to make carbon nanofiber using $ZnCl_2$ as an activator for electro-catalytic oxygen reduction reaction [28]. The resulting carbon nanofiber possesses hetero-elements, but the maximum observed specific surface area was only 721 m^2/g. However, a high surface area and fast mass transfer rate are keys to efficient gas storage and separation applications. Towards this, we have activated spider silk by KOH, and through this, the specific surface area of the resulting spider silk-derived activated-carbon fiber increased by almost four times of the previously reported spider silk-based carbon fibers; hence demonstrated high CO_2 capture performance and CH_4 and H_2 storage capacity.

2. Materials and method

2.1. Preparation of spider silk-derived nanoporous activated carbon fiber (SS-NACF)

Spider silks (SS) were collected from the local area, and after that washed by soaking in distilled water for 24 h at room temperature followed by stirring for 1 h, Fig. S1. The cleaned spider silks were dried at 100 °C for 24 h in the air. Then, the dried spider silks were carbonized by heating at 800 °C for 1 h under N_2 atmosphere. The ramping rate was 5 °C/min, and the N_2 flow rate was 0.15 L/min. Thus, spider silk-derived carbon fiber (SS-CF) was washed with distilled water to remove any foreign substances attached to the sample and dried at 100 °C for 24 h. Finally, the activation process was conducted, and for this, the SS-CF was mixed with potassium hydroxide (KOH) in a ratio of 1:4. Typically, 0.3 g SS-CF was physically mixed with 1.2 g KOH using mortar pastel and activated by using a similar heating condition used for carbonization. After cooling it to room temperature, the obtained product was soaked in 10 wt% HCl and then repeatedly washed with distilled water until neutral pH was observed. Finally, the obtained carbon was vacuum dried at 100 °C for 8 h, and thus obtained carbon was labeled as SS-NACF.

2.2. Physical characterization and gas sorption measurement

The microstructure of the SS-CF and SS-NACF were analyzed using field emission scanning electron microscopy (FE-SEM; MIRA3, TESCAN). Raman spectra were collected using Raman spectrometer (RAMANtouch, Nanophoton) equipped with a laser of 532 nm wavelength. XRD patterns of SS, SS-CF and SS-NACF were recorded using the Rigaku Ultima-IV X-Ray Diffractometer. The elemental composition was examined by X-ray photoelectron spectroscopy (K-Alpha+, Thermo Fisher Scientific). Specific surface area measurements were conducted using N_2 sorption at 77 K with BELSORP-max (BEL, Japan). The pore size distribution was calculated through NLDFT cylindrical model (GCMC) using the adsorption branch of N_2 isotherm. CO_2, CH_4, and H_2 storage application studies were performed in automated Sievert-type high-pressure gas sorption instrument (PCTPro-E&E, Setaram) having a microdoser. Before the gas sorption, about 100 mg sample was activated under a dynamic vacuum at 200 °C for 10 h. CO_2 and CH_4 storage were analyzed at 0 and 25 °C, and 25 bar, while H_2 storage was estimated at − 196 °C and 25 bar. Excess and absolute H_2 uptakes have been estimated based on the method reported earlier [29]. The gas sorption selectivity was estimated using the IAST method. The adsorbent regeneration and recycling were performed using the PCTPro-E&E gas sorption instrument.

3. Results and discussion

KOH activation method was applied to develop high surface area SS-NACF. The activation was performed under an inert atmosphere at 800 °C. The activation temperature was based on the TGA analysis of SS-CF, Fig. S2. In TGA graph, the first mass loss of 5 wt% about 100 °C was due to loss of moisture, and after that, weight loss appeared near 800 °C, and this temperature was chosen for activation of SS-CF. The microstructure of SS-CF and SS-NACF is shown in Fig. 1(a & b). As spider silk has a fibrous microstructure which was well preserved in both SS-CF and SS-NACF, even after carbonization and activation. The fiber surface of SS-CF is relatively smooth, whereas in SS-NACF, a significant roughness after activation can be seen. Such roughness can be ascribed to surface etching during the activation, and it helps in developing porosity.

The SS-CF and SS-NACF have further been analyzed by Raman spectroscopy. The Raman spectra exhibited in Fig. 2(a) shows the D and G bands. The presence of D band at 1340 cm^{-1} is ascribed to crystal defect and disordering in the carbon framework [30,31]. The G band, observed at 1580 cm^{-1}, corresponds to the phonon mode of graphitic sp^2 bonded E_{2g} symmetric carbons [30–32]. The Raman spectra are generally used to access the degree of disordering or graphitization through the ratio of the intensity of D band and G band (I_D/I_G). In this regard, the I_D/I_G ratio for SS-CF and SS-NACF was estimated to be 1.05 and 1.04, respectively, which confirms that both the materials lack long-range ordering and are rather amorphous in nature. It also proves that the degree of graphitization was not altered during the activation process. Further, the XRD patterns of SS-CF and SS-NACF were measured and compared with the pristine SS, Fig. 2(b). SS-CF and SS-NACF exhibited a broad peak at 2θ scale of 22–24° due to amorphous carbon. A sharp peak at 27° for SS and SS-CF was observed due to crystalline SiO_2, a commonly found inorganic material in bio-waste[33]. However, the activated sample demonstrated many sharp peaks of varying intensity due to the presence of SiC and Si, and these are formed through the reduction of SiO_2 by KOH.

The elemental composition and chemical nature of SS-NACF were analyzed by XPS. The survey scan, given in Fig. 3(a), confirmed that SS-NACF consists of C, N, O, and Si. The atomic composition of these four elements was 82% (C), 13.2% (O), 4.2% (Si) and 0.6% (N). The lower atomic percentage of N is caused by its removal from carbonaceous materials due to high-temperature activation. To further understand the chemical nature of elements, the high-resolution C1s, O1s and Si2p XPS spectra were deconvoluted. The C1s spectrum shows four signals and those could be ascribed to C-Si at 284.3 eV, C-C/C═C at 284.8 eV, C-O/C-N at 285.4 eV, and C═O/C═N at 286.5 eV, Fig. 3(b). Similarly, the O1s has three signals at 532.4, 533.4 and 534.6 eV and these could be due to Si-O, O-C and O═C, respectively, Fig. 3(c). The N1s XPS scan, due to its low atomic percentage, is not very smooth; however broad spectrum seen in the binding energy range of 398–404 eV could be due to the

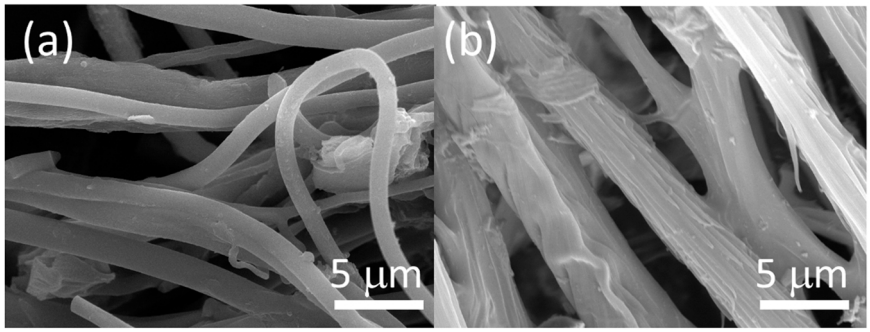

Fig. 1. FE-SEM images of (a) SS-CF and (b) SS-NACF.

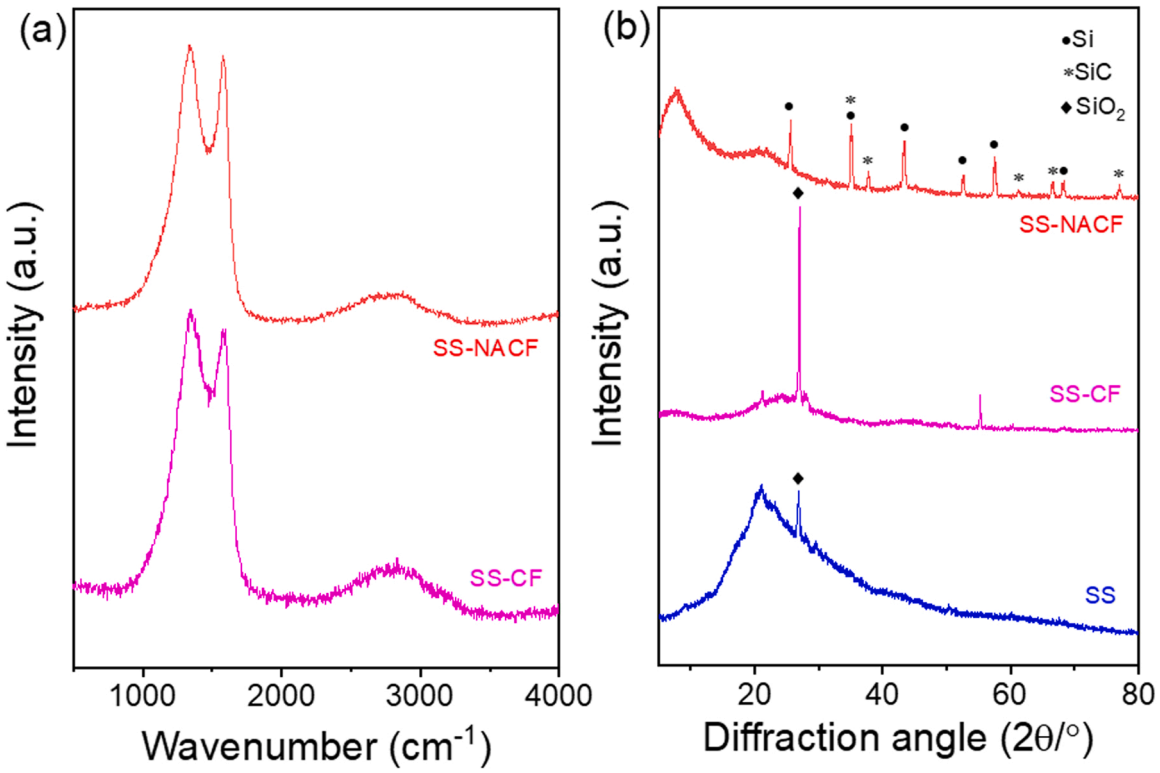

Fig. 2. (a) Raman spectra of SS-CF and SS-NACF, and (b) XRD patterns of SS, SS-CF and SS-NACF.

presence of pyridinic and pyrrolic nitrogen, Fig. 3(d). The Si2p XPS scan shows the three peaks at 103.3, 104.3 and 105.7 eV, and these could be ascribed to elemental Si, Si-C and Si-O linkage, respectively, Fig. 3(e).

Further, SS-CF and SS-NACF were subjected to N_2 sorption analysis to access the porosity. The N_2 isotherm of SS-NACF is shown in Fig. 4(a) while of SS-CF is shown in the inset of Fig. 4(a). The N_2 isotherm of SS-NACF is the combination of type-I and type-IV isotherms, indicating that it has mainly two types of pores. The sharp rise at low pressure confirms the presence of micropores, while an extended knee region in the relative pressure region of 0.1–0.4 and small hysteresis in the higher relative pressure region confirm the presence of mesopores. This was further supported by the pore size distribution calculation performed by GCMC method, Fig. 4(b). The dominant pores in the sample are micropores, but mesopores are also in good proportion. The micropores were of the size of 0.6 and 1.1 nm, while mesopores were found to be centered in the range of 2.2–3.8 nm. The specific surface area was estimated by BET (SSA_{BET}) method in the relative pressure range of 0.12–0.21, Fig. S3 (determined using Rouquerol plot [3]) and it was found to be 2730 m^2/g for SS-NACF in comparison to 44 m^2/g for SS-CF. This ultra-significant rise in the SSA_{BET} is due to surface scratching during the activation process. A similar rise in pore volume, calculated by Gurvich's rule at P/P_0 of 0.99, was also observed. The pore volume for SS-NACF was found to be 1.56 cc/g, while for SS-CF was 0.03 cc/g.

The specific surface area and total pore volume are considered the main textural parameters that influence the gas uptake [34], and the pore hierarchy with a pore size less than 4 nm also plays its role in gas sorption [34]. Thus, the gas molecules get adsorb because of a micropore enhancing van der Waals interaction. In contrast, the mobility increases due to the mesopore (absence of transport limitation), and hence mass transfer rate is high. In addition, the presence of electron-rich elements like N and O enhance the Lewis basic nature of the adsorbent's surface. Due to this, the attraction of Lewis acidic gas "CO_2" with the adsorbent surface can get further enhanced.

As aforementioned, physicochemical features (like high specific surface area, high total pore volume, pore hierarchy, and heteroatoms functionalized surface) of SS-NACF are well-suited for adsorption of Lewis acidic molecule thus it was explored for the CO_2 sorption application. The gas sorption isotherms for CO_2 measured at 0 and 25 °C up to 25 bar are shown in Fig. 5(a). SS-NACF has demonstrated the CO_2 capture capacity of 23.6 and 15.4 mmol/g at 0 and 25 °C, respectively.

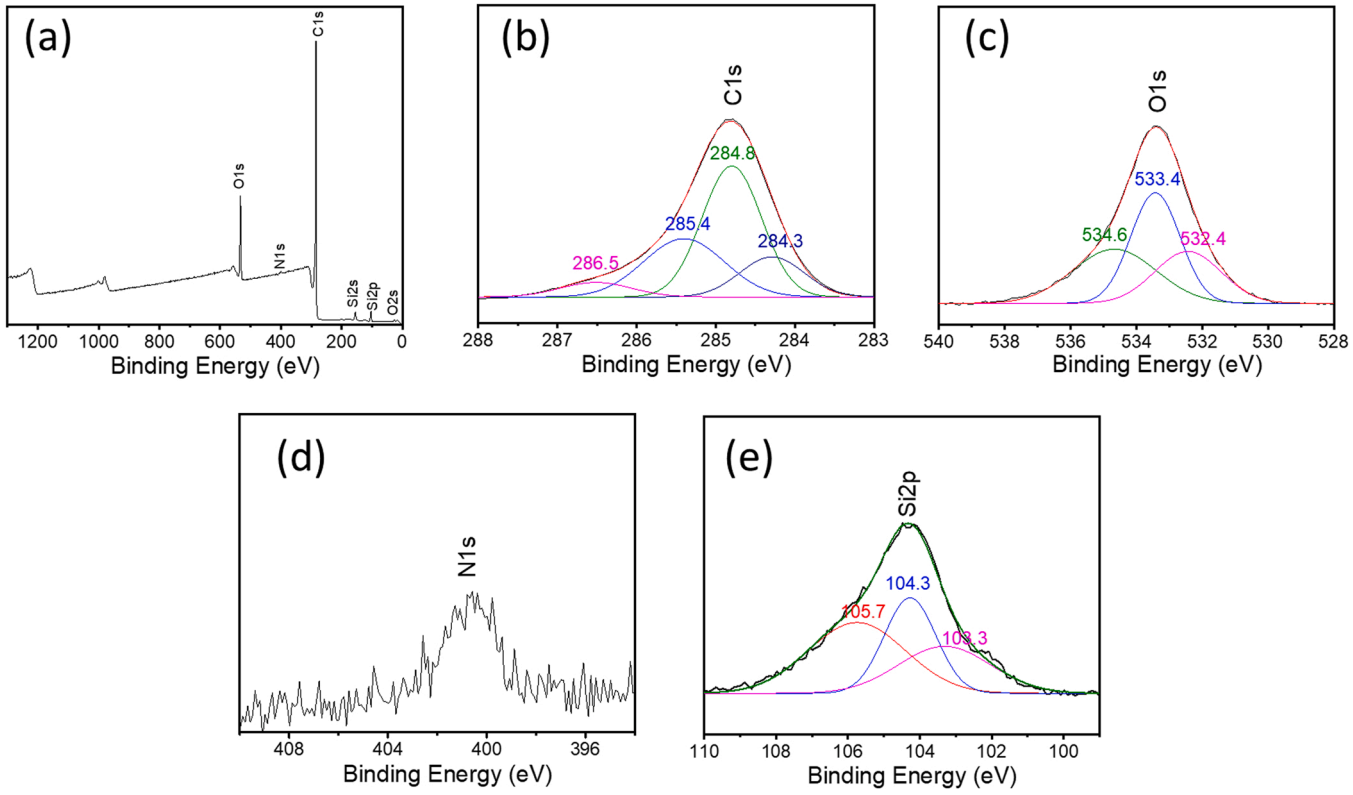

Fig. 3. XPS analysis of SS-NACF; (a) XPS survey scan, (b) C1s XPS scan, (c) O1s XPS Scan, (d) N1s XPS scan and (e) Si2p XPS scan.

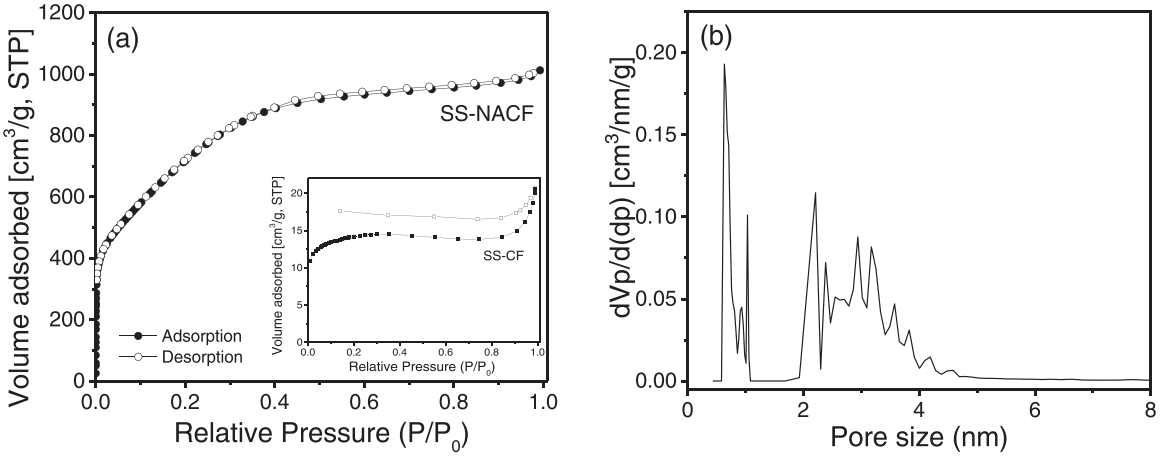

Fig. 4. N_2 sorption study of SS-NACF; (a) Sorption isotherm and (b) pore size distribution. The N_2 sorption isotherm for SS-CF has been provided in the inset of figure (a).

The CO_2 isotherms, up to 25 bar, have not fully attained saturation yet as the uptake continuously increases with pressure. This could be due to the mesoporosity in the sample as the complete filling of these requires high pressure compared to micropore. Moreover, the high CO_2 uptake was also influenced by surface atomic heterogeneity, high surface area and pore volume. Obtained CO_2 uptake of the SS-NACF is comparable to the previously reported carbonaceous adsorbents. For instance, the uptake at 25 °C was higher than CFC54 [35], CFS60 [35], CFCMS [36], AKFs6 [37], CP-AC [38], KOH:CWG-22_850 = 1 [39], K_2CO_3: CWG-22_850 = 4 [39], AC-50 [40] and comparable or less than K-AC [38], A-PC [41], B-PC [42] and PAB-3 [43]. The detailed comparison for uptake capacity can be seen in Table 1. In addition, the isosteric heat of adsorption (Q_{st}) for CO_2 was calculated by Clausius–Clapeyron equation. The Q_{st} for the CO_2 adsorption increases with an increase in surface coverage and the maximum value was found to be 20.5 kJ/mol, Fig. S4. Since the CO_2 isotherms are fully reversible, the regeneration of SS-NACF can be carried out with a minimum energy penalty, hence it can serve as a suitable adsorbent for the pressure swing adsorption method.

SS-NACF was further studied for CH_4 and H_2 storage applications and isotherms are given in Fig. 5(b) and 5(c), respectively. The maximum CH_4 uptakes at 0 and 25 °C were estimated to be 8.6 and 6.4 mmol/g, respectively at 25 bar. Similar to the CO_2 uptake, the CH_4 isotherms were fully reversible although the uptake was not very high, and full saturation was not observed up to 25 bar. Thus, significant CH_4 uptake at 25 °C could be realized above 25 bar (Table. 2). Despite all, the CH_4 uptake performance at 25 °C was higher than CBF-1273-CO_2-1 h [44], KOH0.5TP50 [45], assai MHTC [46], RGC30 [47], RHAC900-SR [48],

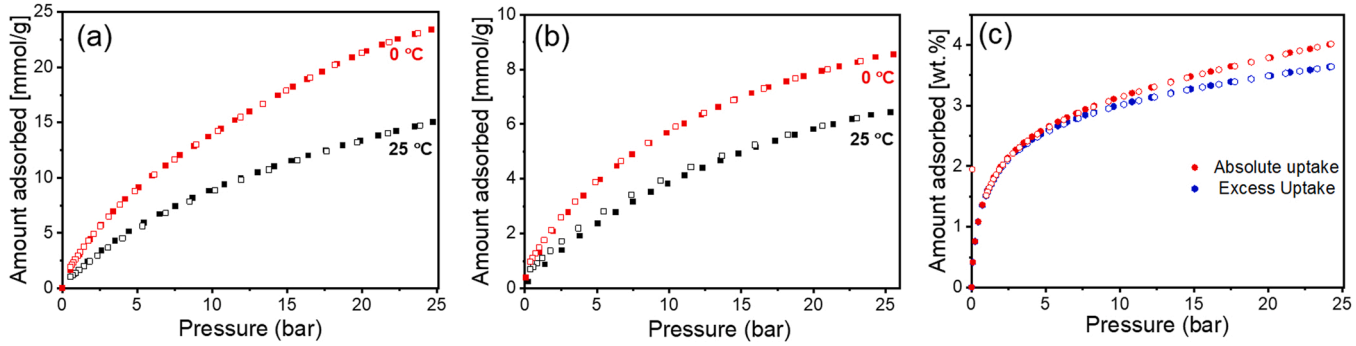

Fig. 5. Gas sorption study of SS-NACF; (a) CO_2 and (b) CH_4 isotherms measured at 0 and 25 °C and 25 bar, (c) H_2 excess and absolute isotherms measured at − 196 °C and 25 bar.

Table 1
CO_2 uptake comparison of SS-NACF with reported adsorbents.

Adsorbents	Uptake (mmol/g)	Pressure/temperature	Reference
SS-NACF	15.4	25 bar/25 °C	This work
CFC54	14.4	40 bar/25 °C	[35]
CFS60	15.3	40 bar/25 °C	[35]
CFCMS	~11.1	58 bar/25 °C	[36]
AKFs6	9.0	15 bar/25 °C	[37]
CP-AC	14.3	35 bar/25 °C	[38]
K-AC	18.4	35 bar/25 °C	[38]
KOH:CWG-22_850 = 1	14.9	35 bar/25 °C	[39]
K_2CO_3:CWG-22_850 = 4	11.2	35 bar/25 °C	[39]
AC-50	9.0	30 bar/25 °C	[40]
A-PC	21.1	30 bar/23 °C	[41]
B-PC	26.0	30 bar/25 °C	[42]
PAB-3	19.3	30 bar/25 °C	[43]

Table 2
CH_4 uptake comparison of SS-NACF with reported adsorbents.

Adsorbents	Uptake (mmol/g)	Pressure/temperature	Reference
SS-NACF	6.4	25 bar / 25 °C	This work
CBF-1273-CO_2-1 h	3.5	10 bar / 25 °C	[44]
KOH0.5TP50	5.1	40 bar / 25 °C	[45]
MHTC	5.0	40 bar / 25 °C	[46]
RGC30	6.1	35 bar / 25 °C	[47]
RHAC900-SR	4.3	35 bar / 25 °C	[48]
Cu–N-MC-0.5	5.0	50 bar/25 °C	[49]
ADPC05	6.4	35 bar / 25 °C	[50]
monolith NCM	13.3	100 bar / 25 °C	[51]

Cu–N-MC-0.5 [49] and comparable to ADPC05 [50] and lower than monolith NCM [51]. The maximum Q_{st} for CH_4 adsorption was calculated to 19.6 kJ/mol, Fig. S4. Excess hydrogen uptake of SS-NACF up to 25 bar was measured at − 196 °C, and shown in Fig. 5(c). The excess and absolute hydrogen storage capacity were estimated to be 3.7 wt% and 4.1 wt%, respectively at 25 bar, − 196 °C with fully reversible sorption. The rapid initial (low-pressure region) increase of uptake indicates preferential H_2 adsorption on SS-NACF due to the existence of a micropore and heteroatoms (oxygen-rich) functionalized surface [51]. In the higher-pressure region, the multi-layer adsorption in the pore (mesopore filling) are only observed [52]. The excess H_2 uptake comparison with the reported superior adsorbents like C1000 [53], FF-4600 [54], PPY2 [55] and PPY4800 [56] is provided in Table 3.

Due to its sustainability compared to other methods, the adsorbent-based gas separation (e.g. PSA, pressure swing adsorption) is getting preference [57]. The selective uptake and adsorption recycling performance define the suitability of the adsorbent materials towards particular applications [42,58]. Towards this, CO_2 vs. N_2 ($S_{CO2/N2}$), CO_2 vs. CH_4 ($S_{CO2/CH4}$) and CH_4 vs. N_2 ($S_{CH4/N2}$) selectivities have been calculated by applying Ideal Adsorb Solution Theory (IAST) method from single gas component, Fig. 6(a-c). In the flue gas, the composition of CO_2 and N_2 is about 15:85 and with this composition [59], the maximum $S_{CO2/N2}$ selectivity of 13 was achieved at 0 °C and 25 bar. $S_{CO2/N2}$ decreased to 8 at 25 °C, which could be ascribed to a decrease in uptake caused by the adsorption thermodynamic at the higher temperature. $S_{CO2/CH4}$ was calculated using the CO_2 and CH_4 composition of 10:90, at 0 °C, it was found to be 3.8, and at 25 °C it was 3.4. The $S_{CO2/CH4}$ keeps increasing with pressure loading, which could be due to the increase in the Q_{st} for CO_2 adsorption with the increase in the surface coverage, as seen above. The $S_{CH4/N2}$ values with CH_4 and N_2 composition of 80:20 were calculated to be 3.9 and 2.4 at 0 and 25 °C, respectively. Further, the regeneration and cycling performance were tested for CO_2 and CH_4 at 25 °C and 25 bar, Fig. 6(d & e). The uptake performance remains almost the same, with just a negligible decrease in uptake for both CO_2 and CH_4 after 10 adsorption-desorption cycles. This confirms the easy regeneration and recyclability of the SS-NACF and makes it a suitable adsorbent for the pressure swing adsorption method.

Table 3
Excess H_2 uptake comparison of SS-NACF with reported adsorbents.

Adsorbents	Uptake (wt%)	Pressure/temperature	Reference
SS-NACF	3.7	25 bar / − 196 °C	This work
C1000	3.3	17.9 bar / − 196 °C	[53]
FF-4600	4.6	20 bar / − 196 °C	[54]
PPY2	3.3	20 bar / − 196 °C	[55]
PPY4800	4.9	20 bar / − 196 °C	[56]

4. Conclusions

In summary, the KOH activation of spider silk (natural biomaterial) led to the development of naturally (heteroatoms) doped activated carbon fibers with high surface area. Due to its high porosity and pore hierarchy and cooperative binding assistance extended by the surface heteroatoms, the activated carbon fibers showed a high gas storage capacity and easy regeneration, and cycling performance. As the natural biomaterials consist of the heteroatoms functionalized building blocks, the adopted approach to develop the SS-NACF can be extended to other natural biomaterials having fibrous microstructure to convert into the heteroatom functionalized activated fibrous carbon needed for advanced energy and environmental application. Moreover, this approach, compared to the conventional way, is less time-consuming and more sustainable for developing the high surface area activated carbon fibers.

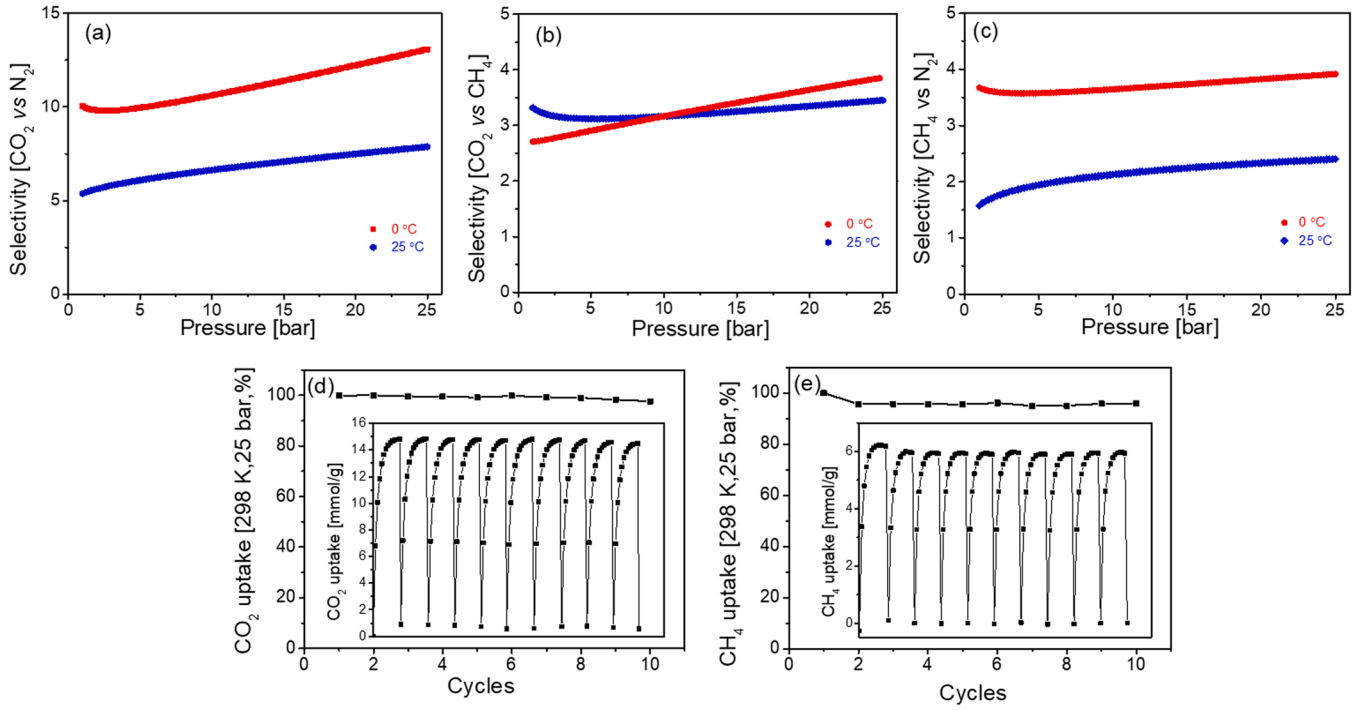

Fig. 6. Gas sorption selectivity calculated by IAST method of SS-NACF; (a) CO_2 vs N_2, (b) CO_2 vs CH_4, and (c) CH_4 vs N_2. (d) and (e) are CO_2 and CH_4 adsorption cycles, respectively.

Declaration of Competing Interest

The authors declare that they have no known competing financial interests or personal relationships that could have appeared to influence the work reported in this paper.

Data Availability

Data will be made available on request.

Acknowledgements

This research was funded by the National Research Foundation of Korea (NRF), Government of Korea (MSI) (2019M3E6A1103980, 2020M2D2A1A02069267). R. M. acknowledges the Brain Pool Program funded by the National Research Foundation of Korea (Grant number: 2019H1D3A1A01071069). The authors also thank the Cooperative Equipment Center of KOREATECH for assistance with XPS analysis. This paper was also supported by "Regional Innovation Strategy (RIS)" through the National Research Foundation of Korea (NRF) funded by the Ministry of Education (MOE)(2021RIS-004).

Author statement

H.O. initiated the experiments. R. M. and H. O. proposed the work and did the project management. R. M. synthesized the samples. Y. N., R. M., and H. O. performed the application study, analyzed the data, and wrote the manuscript, and H. O. did the final editing. All authors read the final manuscript, revised it, and gave consent to the submission.

Appendix A. Supporting information

Supplementary data associated with this article can be found in the online version at doi:10.1016/j.jcou.2023.102401.

References

[1] H. Wang, Y. Shao, S. Mei, Y. Lu, M. Zhang, J.-K. Sun, K. Matyjaszewski, M. Antonietti, J. Yuan, Polymer-derived heteroatom-doped porous carbon materials, Chem. Rev. 120 (2020) 9363–9419.
[2] R. Muhammad, S. Kim, J. Park, M. Jung, M.E. Lee, J. Chung, H. Jang, H. Oh, Chemical affinity-assisted H_2 isotope separation using Ca-rich onion-peel-derived nanoporous carbon composite, Mater. Chem. Front. 5 (2021) 8018–8024.
[3] S.N. Talapaneni, J.H. Lee, S.H. Je, O. Buyukcakir, T.-W. Kwon, K. Polychronopoulou, J.W. Choi, A. Coskun, Chemical blowing approach for ultramicroporous carbon nitride frameworks and their applications in gas and energy storage, Adv. Funct. Mater. 27 (2017) 1604658.
[4] Z. Zhang, Z.P. Cano, D. Luo, H. Dou, A. Yu, Z. Chen, Rational design of tailored porous carbon-based materials for CO_2 capture, J. Mater. Chem. A 7 (2019) 20985–21003.
[5] M.R. Benzigar, S.N. Talapaneni, S. Joseph, K. Ramadass, G. Singh, J. Scaranto, U. Ravon, K. Al-Bahily, A. Vinu, Recent advances in functionalized micro and mesoporous carbon materials: synthesis and applications, Chem. Soc. Rev. 47 (2018) 2680–2721.
[6] G. Singh, J. Lee, A. Karakoti, R. Bahadur, J. Yi, D. Zhao, K. Al-Bahily, A. Vinu, Emerging trends in porous materials for CO_2 capture and conversion, Chem. Soc. Rev. 49 (2020) 4360–4404.
[7] H.A. Patel, J. Byun, C.T. Yavuz, Carbon dioxide capture adsorbents: chemistry and methods, ChemSusChem 10 (2017) 1303.
[8] G. Nazir, A. Rehman, S.-J. Park, Sustainable N-doped hierarchical porous carbons as efficient CO_2 adsorbents and high-performance supercapacitor electrodes, J. CO_2 Util. 42 (2020), 101326.
[9] R. Muhammad, M. Chaudhary, P. Mohanty, Harnessing electron-rich framework in cyclophosphazene derived hybrid nanoporous materials for organocatalytic C-C bond formation and gas sorption applications, J. CO_2 Util. 25 (2018) 302–309.
[10] R. Muhammad, P. Mohanty, Cyclophosphazene-based hybrid nanoporous materials as superior metal-free adsorbents for gas sorption applications, Langmuir 34 (2018) 2926–2932.
[11] M.F. Hassan, M.A. Sabri, H. Fazal, A. Hafeez, N. Shezad, M. Hussain, Recent trends in activated carbon fibers production from various precursors and applications—a comparative review, J. Anal. Appl. Pyrolysis 145 (2020), 104715.
[12] Z. Li, D. Guo, Y. Liu, H. Wang, L. Wang, Recent advances and challenges in biomass-derived porous carbon nanomaterials for supercapacitors, Chem. Eng. J. 397 (2020), 125418.
[13] H.D. Asfaw, R. Gond, A. Kotronia, C.-W. Tai, R. Younesi, Bio-derived hard carbon nanosheets with high rate sodium-ion storage characteristics, Sustain. Mater. Technol. 32 (2022), e00407.
[14] Y. Lv, L. Gan, M. Liu, W. Xiong, Z. Xu, D. Zhu, D.S. Wright, A self-template synthesis of hierarchical porous carbon foams based on banana peel for supercapacitor electrodes, J. Power Sources 209 (2012) 152–157.
[15] P. Hao, Z. Zhao, Y. Leng, J. Tian, Y. Sang, R.I. Boughton, C.P. Wong, H. Liu, B. Yang, Graphene-based nitrogen self-doped hierarchical porous carbon aerogels

derived from chitosan for high performance supercapacitors, Nano Energy 15 (2015) 9–23.
[16] L. Han, P. Zhang, L. Li, S. Lu, B. Su, X. An, Z. Lei, Nitrogen-containing carbon nano-onions-like and graphene-like materials derived from biomass and the adsorption and visible photocatalytic performance, Appl. Surf. Sci. 543 (2021), 148752.
[17] K.-L. Chiu, D.H.L. Ng, Synthesis and characterization of cotton-made activated carbon fiber and its adsorption of methylene blue in water treatment, Biomass-.-. Bioenerg. 46 (2012) 102–110.
[18] S. Wang, Y.-R. Lee, Y. Won, H. Kim, S.-E. Jeong, B.W. Hwang, A.R. Cho, J.-Y. Kim, Y.C. Park, H. Nam, D.-H. Lee, H. Kim, S.-H. Jo, Development of high-performance adsorbent using KOH-impregnated rice husk-based activated carbon for indoor CO_2 adsorption, Chem. Eng. J. 437 (2022), 135378.
[19] R. Awad, A.H. Mamaghani, Y. Boluk, Z. Hashisho, Synthesis and characterization of electrospun PAN-based activated carbon nanofibers reinforced with cellulose nanocrystals for adsorption of VOCs, Chem. Eng. J. 410 (2021), 128412.
[20] X. Li, L. Zhao, T. He, M. Zhang, Z. Wang, B. Zhang, X. Weng, Highly conductive, hierarchical porous ultra-fine carbon fibers derived from polyacrylonitrile/polymethylmethacrylate/needle coke as binder-free electrodes for high-performance supercapacitors, J. Power Sources 521 (2022), 230943.
[21] W.-H. Kuan, Y.-S. Hu, C.-Y. Chiu, K.-Y. Hung, S.-S. Chou, Microwave-catalyzed conversion of phenolic resin waste to activated carbon and its applications for removing ammonium from water, Catalysts 11 (2021) 783.
[22] Y.-H. Wang, S. Bayatpour, X. Qian, B. Frigo-Vaz, P. Wang, Activated carbon fibers via reductive carbonization of cellulosic biomass for adsorption of nonpolar volatile organic compounds, Colloid Surf. A-Physicochem. Eng. Asp. 612 (2021), 125908.
[23] D. Xinhui, C. Srinivasakannan, W. Xin, W. Fei, L. Xinyi, Synthesis of activated carbon fibers from cotton by microwave induced H_3PO_4 activation, J. Taiwan Inst. Chem. Eng. 70 (2017) 374–381.
[24] N.H. Phan, S. Rio, C. Faur, L.L. Coq, P.L. Cloirec, T.H. Nguyen, Production of fibrous activated carbons from natural cellulose (jute, coconut) fibers for water treatment applications, Carbon 44 (2006) 2569–2577.
[25] Y. Huang, L. Peng, Y. Liu, G. Zhao, J.Y. Chen, G. Yu, Biobased nano porous active carbon fibers for high-performance supercapacitors, ACS Appl. Mater. Interfaces 8 (2016) 15205–15215.
[26] L. Zhang, L.-Y. Tu, Y. Liang, Q. Chen, Z.-S. Li, C.-H. Li, Z.-H. Wang, W. Li, Coconut-based activated carbon fibers for efficient adsorption of various organic dyes, RSC Adv. 8 (2018) 42280–42291.
[27] A. Rising, M. Widhe, J. Johansson, M. Hedhammar, Spider silk proteins: recent advances in recombinant production, structure–function relationships and biomedical applications, Cell. Mol. Life Sci. 68 (2011) 169–184.
[28] L. Zhou, P. Fu, X. Cai, S. Zhou, Y. Yuan, Naturally derived carbon nanofibers as sustainable electrocatalysts for microbial energy harvesting: a new application of spider silk, Appl. Catal. B-Environ. 188 (2016) 31–38.
[29] M. Schlichtenmayer, B. Streppel, M. Hirscher, Hydrogen physisorption in high SSA microporous materials – a comparison between AX-21_33 and MOF-177 at cryogenic conditions, Int. J. Hydrog. Energy 36 (2011) 586–591.
[30] E. Frank, L.M. Steudle, D. Ingildeev, J.M. Spörl, M.R. Buchmeiser, Carbon fibers: precursor systems, processing, structure, and properties, Angew. Chem. Int. Ed. 53 (2014) 5262–5298.
[31] A.C. Ferrari, J. Robertson, Interpretation of Raman spectra of disordered and amorphous carbon, Phys. Rev. B 61 (2000) 14095–14107.
[32] R. Muhammad, N.F. Attia, S. Cho, J. Park, M. Jung, J. Chung, H. Oh, Exploitation of surface heterogeneity and textural properties in nanoporous carbon fabrics for efficient iodine capture, Thin Solid Films 706 (2020), 138049.
[33] B. Xue, L. Jin, Z. Chen, Y. Zhu, Z. Wang, X. Liu, X. Wang, The template effect of silica in rice husk for efficient synthesis of the activated carbon based electrode material, J. Alloy. Compd. 789 (2019) 777–784.
[34] P.M.S. Sai, K. Krishnaiah, Development of the pore-size distribution in activated carbon produced from coconut shell char in a fluidized-bed reactor, Ind. Eng. Chem. Res. 44 (2005) 51–60.
[35] D. Cazorla-Amorós, J. Alcañiz-Monge, A. Linares-Solano, Characterization of activated carbon fibers by CO_2 adsorption, Langmuir 12 (1996) 2820–2824.
[36] T.D. Burchell, R.R. Judkins, A novel carbon fiber based material and separation technology, Energy Conv. Manag. 38 (1997) S99–S104.
[37] G. Conte, S. Stelitano, A. Policicchio, F.D. Minuto, V. Lazzaroli, F. Galiano, R. G. Agostino, Assessment of activated carbon fibers from commercial Kevlar® as nanostructured material for gas storage: effect of activation procedure and adsorption of CO_2 and CH_4, J. Anal. Appl. Pyrolysis 152 (2020), 104974.
[38] R. Ahmadi, M. Ardjmand, A. Rashidi, M. Rafizadeh, High performance novel nanoadsorbents derived - natural cellulose fibers for superior CO_2 adsorption and CO_2 / CH_4 separation, Energy Sources Part A (2020) 1–19l.
[39] J. Sreńscek-Nazzal, K. Kiełbasa, Advances in modification of commercial activated carbon for enhancement of CO_2 capture, Appl. Surf. Sci. 494 (2019) 137–151.
[40] I.S. Ismail, N.A. Rashidi, S. Yusup, Production and characterization of bamboo-based activated carbon through single-step H_3PO_4 activation for CO_2 capture, Environ. Sci. Pollut. Res. 29 (2022) 12434–12440.
[41] A.S. Jalilov, G. Ruan, C.-C. Hwang, D.E. Schipper, J.J. Tour, Y. Li, H. Fei, E. L. Samuel, J.M. Tour, Asphalt-derived high surface area activated porous carbons for carbon dioxide capture, ACS Appl. Mater. Interfaces 7 (2015) 1376–1382.
[42] Y. Li, G. Ruan, A.S. Jalilov, Y.R. Tarkunde, H. Fei, J.M. Tour, Biochar as a renewable source for high-performance CO_2 sorbent, Carbon 107 (2016) 344–351.
[43] I.S. Ismail, G. Singh, P. Smith, S. Kim, J.-H. Yang, S. Joseph, S. Yusup, M. Singh, V. Bansal, S.N. Talapaneni, A. Vinu, Oxygen functionalized porous activated biocarbons with high surface area derived from grape marc for enhanced capture of CO_2 at elevated-pressure, Carbon 160 (2020) 113–124.
[44] A. Arami-Niya, T.E. Rufford, Z. Zhu, Nitrogen-doped carbon foams synthesized from banana peel and zinc complex template for adsorption of CO_2, CH_4, and N_2, Energy Fuels 30 (2016) 7298–7309.
[45] A. Arami-Niya, T.E. Rufford, Z. Zhu, Activated carbon monoliths with hierarchical pore structure from tar pitch and coal powder for the adsorption of CO_2, CH_4 and N_2, Carbon 103 (2016) 115–124.
[46] O.F. Cruz Jr., J. Silvestre-Albero, M.E. Casco, D. Hotza, C.R. Rambo, Activated nanocarbons produced by microwave-assisted hydrothermal carbonization of Amazonian fruit waste for methane storage, Mater. Chem. Phys. 216 (2018) 42–46.
[47] M.E. Casco, M. Martínez-Escandell, E. Gadea-Ramos, K. Kaneko, J. Silvestre-Albero, F. Rodríguez-Reinoso, High-pressure methane storage in porous materials: are carbon materials in the pole position? Chem. Mater. 27 (2015) 959–964.
[48] J.-H. Lee, Y.-J. Heo, S.-J. Park, Effect of silica removal and steam activation on extra-porous activated carbons from rice husks for methane storage, Int. J. Hydrog. Energy 43 (2018) 22377–22384.
[49] K. Ramadass, K.S. Lakhi, C.I. Sathish, A.M. Ruban, R. Bahadur, G. Singh, H. S. Gujral, M. Al-Abri, Ala'a H. Al-Muhtaseb, E. Tavakkoli, J. Yi, A. Karakoti, A. Vinu, Copper nanoparticles decorated N-doped mesoporous carbon with bimodal pores for selective gas separation and energy storage applications, Chem. Eng. J. 431 (2022), 134056.
[50] S. Stelitano, G. Conte, A. Policicchio, A. Aloise, G. Desiderio, R.G. Agostino, Low pressure methane storage in pinecone-Derived activated carbons, Energy Fuels 32 (2018) 10891–10897.
[51] A. Memetova, I. Tyagi, R.R. Karri, Suhas, N. Memetov, A. Zelenin, R. Stolyarov, A. Babkin, V. Yagubov, I. Burmistrov, A. Tkachev, V. Bogoslovskiy, G. Shigabaeva, E. Galunin, High-density nanoporous carbon materials as storage material for Methane: a value-added solution, Chem. Eng. J. 433 (2022), 134608.
[52] C. Sathish, S. Premkumar, X. Chu, X. Yu, M.B.H. Breese, M. Al-Abri, A.'a H. Al-Muhtaseb, A. Karakoti, J. Yi, A. Vinu, Microporous carbon nitride (C3N5.4) with Tetrazine based molecular structure for efficient adsorption of CO_2 and water, Angew. Chem. Int. Ed. 60 (2021) 21242.
[53] W. Wang, D. Yuan, Mesoporous carbon originated from non-permanent porous MOFs for gas storage and CO_2/CH_4 separation, Sci. Rep. 4 (2014) 5711.
[54] L.S. Blankenship, R. Mokaya, Cigarette butt-derived carbons have ultra-high surface area and unprecedented hydrogen storage capacity, Energy Environ. Sci. 10 (2017) 2552–2562.
[55] B. Adeniran, R. Mokayan, Compactivation: a mechanochemical approach to carbons with superior porosity and exceptional performance for hydrogen and CO_2 storage, Nanomater Energy 16 (2015) 173–185.
[56] N. Balahmar, R. Mokaya, Pre-mixed precursors for modulating the porosity of carbons for enhanced hydrogen storage: towards predicting the activation behaviour of carbonaceous matter, J. Mater. Chem. A 7 (2019) 17466–17479.
[57] S. Sircar, T.C. Golden, M.B. Rao, Activated carbon for gas separation and storage, Carbon 34 (1) (1996) 1–12.
[58] R. Muhammad, P. Rekha, P. Mohanty, Aminal linked inorganic–organic hybrid nanoporous materials (HNMs) for CO_2 capture and H_2 storage applications, RSC Adv. 6 (2016) 17100–17105.
[59] W. Lu, D. Yuan, J. Sculley, D. Zhao, R. Krishna, H.-C. Zhou, Sulfonate-grafted porous polymer networks for preferential CO_2 adsorption at low pressure, J. Am. Chem. Soc. 133 (2011) 18126–18129.